# Strongly nonlinear effects on determining internal solitary wave parameters from remote sensing signatures

**Tao Xu[1], Xu Chen[2*], Qun Li[3], Xiao He[2], Jing Wang[1], and Jing Meng[2]**

[1] School of Physics and Optoelectronic Engineering, Ocean University of China, Qingdao, China.

[2] Key Laboratory of Physical Oceanography, Ocean University of China and Qingdao National Laboratory for Marine Science and Technology, Qingdao, China.

[3] MNR Key Laboratory for Polar Science, Polar Research Institute of China, Shanghai, China.

Corresponding author: Xu Chen (chenxu001@ouc.edu.cn)

**Key Points:**

- The relationship between the surface and internal characteristics of internal solitary waves is established in laboratory experiments.
- A fully nonlinear model is used to determine wave parameters from surface features and has been well verified.
- Stratification conditions differentiate the relationship between remote sensing signatures and wave parameters in deep and shallow seas.

## Abstract

The inversion of remote sensing signatures of internal solitary waves (ISWs) can retrieve dynamic characteristics in the ocean interior. The ubiquitous large-amplitude ISWs limit the weakly nonlinear methods commonly used to retrieve wave parameters. We establish the relationship between surface features and internal characteristics of ISWs in laboratory experiments through the correspondence of the remote sensing signatures and the surface velocities of ISWs. The results show that the strong nonlinearity makes the solution of wave-induced velocity inseparable, and ISW theories under the weakly nonlinear assumption are inappropriate to describe strongly nonlinear ISWs from the surface. Therefore, the fully nonlinear model Dubreil–Jacotin–Long equation is used in the retrievals and has been well verified in both the laboratory and oceans. Mooring observations and the model show that stratification conditions differentiate the relationship between remote sensing signatures and ISW parameters in deep and shallow seas.



## Plain Language Summary

Internal solitary waves (ISWs), as nonlinear internal waves, play an essential role in oceanic human activities and ocean mixing. The surface current induced by ISWs can create rough and smooth regions on the sea surface due to the modulated roughness, hence presenting alternating bright and dark stripes in satellite images. Satellites can observe ISWs over a wide range via surface manifestations, and the internal dynamics can be calculated from surface features using retrieval methods. However, the availability of retrieval methods still needs to be verified, facing the difficulty of matching mooring observations and satellite images of the same ISW in a short time interval. According to the proportional relation of remote sensing signatures and wave-induced velocities, this study establishes the relationship between surface features and internal characteristics of ISWs in laboratory experiments. Different from the weakly nonlinear models used in previous studies, a fully nonlinear model is used in the retrieval and has achieved good results in the laboratory and oceans. The model and mooring observations show the critical role of stratifications in the retrieval. This work provides a reliable dynamics model for the inversion of remote sensing signatures of ISWs into characteristics in the ocean interior.

## 1 Introduction

Internal solitary waves (ISWs) are widespread in marginal seas (Jackson, 2007), and are usually generated due to the nonlinear steepening of internal tides (Ramp et al., 2010). With large amplitudes and strong currents, ISWs can damage ocean engineering and underwater vehicles (Huang et al., 2016; Klymak et al., 2006; Osborne & Burch, 1980). The breaking of ISWs during shoaling can cause enhanced mixing, change underwater acoustic transmission, and affect nearshore ecosystems (Alford et al., 2015; Chiu et al., 2013; Moum et al., 2003; Wang et al., 2007).

ISWs create convergence and divergence zones on the sea surface, resulting in rough and smooth regions on the sea surface due to the modulated roughness (Lenain & Pizzo, 2021; Yue et al., 2022) and presenting alternating bright and dark stripes in satellite images. The characteristics of ISWs, such as wave crest length, propagation direction and propagation speed can be acquired from the images (Jackson, 2007; Liu et al., 2014; Zhao et al., 2004), while other essential characteristics such as amplitude and wavelength cannot be directly obtained. Therefore, retrieval methods of ISW parameters based on physical models have been proposed, which establish the relation between the remote sensing characteristics and other wave parameters in the ocean interior. A variety of retrieval methods were established using different ISW theories and wave-induced velocity calculation methods.

A retrieval method based on the Korteweg-de Vries (KdV) equation was first proposed (Small et al., 1999; Zheng et al., 2001) and widely used for determining ISW parameters (Fan et al., 2015; Gong et al., 2021; Hong et al., 2016; Phaniharam et al., 2020; Wang et al., 2022; Xie et al., 2022). This method established the relation between the ISW distribution of stripes and their wavelengths. Then, the waveform and amplitude could be determined with stratifications. Retrieval methods using the Joseph–Kubota–Ko–Dobbs (JKKD) equation for finite depth (Pan et al., 2007), the Benjamin–Ono (BO) equation for infinite depth (Chen et al., 2011; C. Wang et al., 2019) and the extended KdV (eKdV) equation (Jia et al., 2019; Xue et al., 2013) were also proposed to analyze satellite images similarly. These methods above were based on a weakly nonlinear assumption, which assumes that the amplitude of ISWs is small compared with the intrinsic vertical scale (Choi & Camassa, 1999). Under the weakly nonlinear assumption, the solution of the wave-induced velocity is considered to be separable in the horizontal and vertical directions.

However, strongly nonlinear ISWs that do not satisfy the weak nonlinearity assumption account for a large proportion of in-situ oceanic observations. (Chang et al., 2021; Huang et al., 2022; Stanton & Ostrovsky, 1998; Yang et al., 2021). Although weakly nonlinear theories have been used outside their formal range of validity in some cases (Helfrich & Melville, 2006), for a detailed description of the dynamics of large-amplitude ISWs observed in the real ocean, theoretical models with strong nonlinearity are needed (Vlasenko et al., 2000). The Miyata–Choi–Camassa (MCC) equation, a fully nonlinear theory of long waves was proposed and agreed well with laboratory experiments (Camassa et al., 2006; Kodaira et al., 2016). Meanwhile, without any assumptions, the fully nonlinear Dubriel–Jacotin–Long (DJL) equation has been applied effectively in the laboratory and the ocean (Camassa et al., 2018; Chang et al., 2021; Lien et al., 2014; Luzzatto-Fegiz & Helfrich, 2014). Different from the separable solution of velocity under weakly nonlinear approximation, the solution cannot be separated with strong nonlinearity. To date, strongly nonlinear effects on the retrievals of wave parameters have not been fully considered in the following two aspects: (1) the calculation of wave-induced velocities and (2) the applicability of ISW theories. The adequate modeling of ISW dynamics should be determined in the retrieval, as mentioned by Romeiser and Graber (2015).

To address the difficulty of matching mooring observations and satellite images of the same ISW in a short time interval, this paper establishes the relationship between surface features and internal characteristics of ISWs in laboratory experiments. Then the strongly nonlinear effects on retrieving ISW parameters are evaluated in terms of wave-induced velocities and ISW theories. Finally, we assess the retrieval of wave parameters in different oceanic environments.

## 2 Methodology

### 2.1 Laboratory experiments and data processing

Experiments are conducted in the Key Laboratory of Physical Oceanography, Ocean University of China. Two layers of fluid with thickness of $h_1$ and $h_2$ and densities of 1020kg/m$^3$ and 1040kg/m$^3$ are injected into the tank. The depth ratio of the lower and upper layers $h_2/h_1$vary from 3 to 10. The waves are generated by the lock–release method (Sutherland et al., 2015), with nondimensional amplitudes $\eta_0/h_1$ ranging from 0.18 to 2.50; see Table S1 in the supporting information for the detailed conditions. Two synchronous charge coupled device

(CCD) cameras with bandpass filters are set in front of the tank. The wave-induced velocity is measured by particle image velocity (PIV) (Thielicke & Stamhuis, 2014; S. Wang et al., 2019), and the waveform $\eta(x)$ is determined by identifying the depth where the maximal vertical density gradient is located using the synthetic Schlieren technique (Dalziel et al., 2007). The wavelength of ISWs is defined as

$$L_w = \frac{1}{2\eta_0} \int_{-\infty}^{\infty} \eta(x)\, \mathrm{d}x. \tag{1}$$

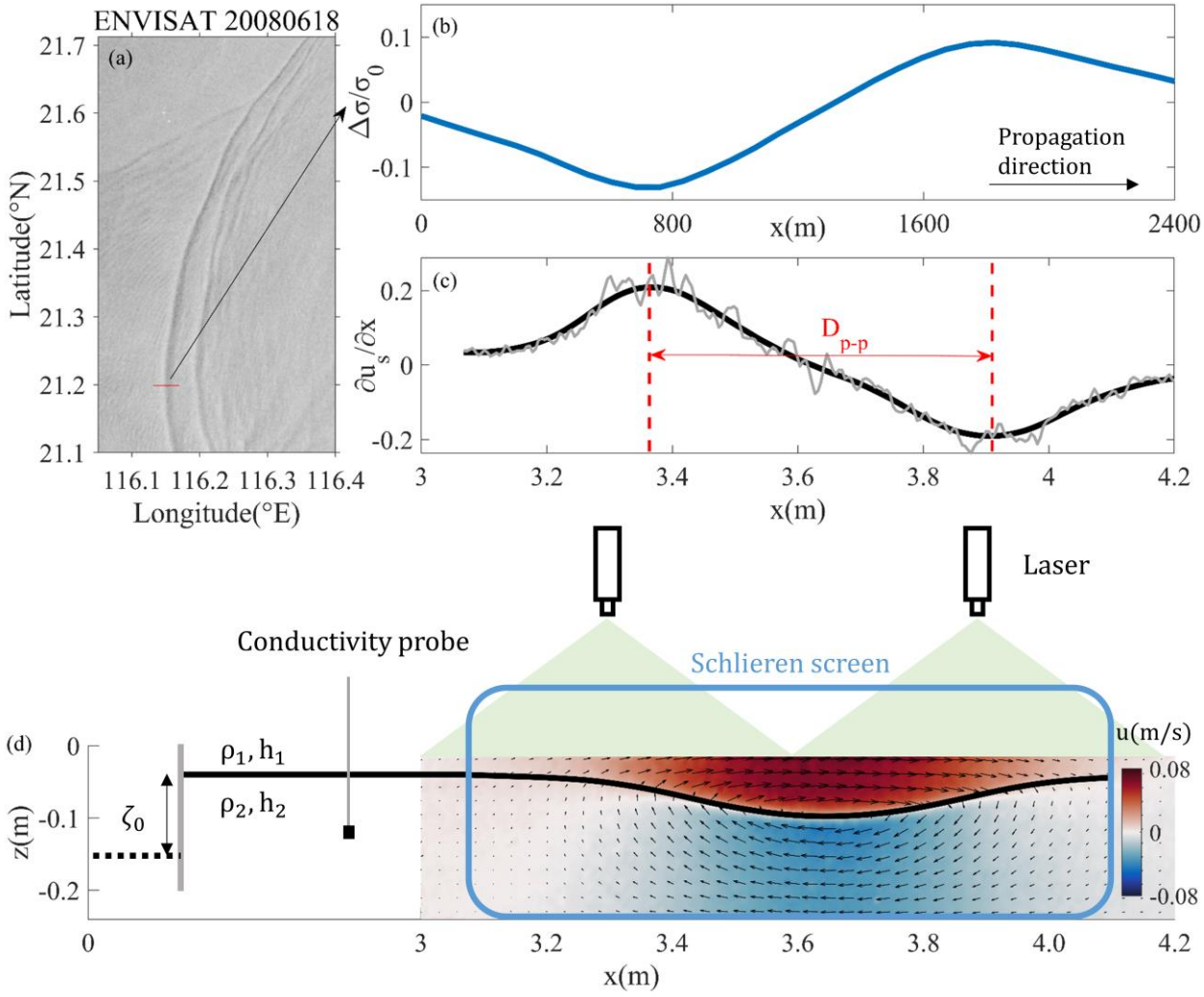


**Figure 1.** Schematic of experiments. (a) ISWs captured by ENVISAT on June 18, 2008, UTC. (b) Relative image intensity along the direction of wave propagation (the red line in subfigure a).

(c) The surface horizontal velocity divergence of the ISW in the laboratory experiment. The gray and black lines present the original and smoothed results, respectively. Red dashed lines indicate the horizontal position corresponding to the maximum and minimum values. (d) Schematic diagram of the experiment in the same case as subfigure c.

We consider the radar imaging theory which describes the influence of surface currents on remote sensing imaging (Alpers, 1985) as

$$\frac{\Delta\sigma}{\sigma_0} \propto -\frac{\partial u_s}{\partial x}, \tag{2}$$

where $\Delta\sigma = \sigma - \sigma_0$ denotes the deviation of the normalized radar cross-section intensity from its mean value, $u_s$ denotes the velocities of surface currents, and the $x$ direction is defined as the direction of wave propagation. This means that the signal in satellite images (Figure 1a and 1b) can be calculated from the divergence of surface velocities induced by ISWs in an equilibrium and steady environment. The distance between the positive peak and the adjacent negative peak $D_{p-p}$ in satellite images of ISWs is less affected by winds in most cases (Brandt et al., 1999; Xue et al., 2013). Hence the peak-to-peak distance $D_{p-p}$ is chosen to characterize the surface features of ISWs in our experiments (Figure 1c and 1d), which is expressed as

$$D_{p-p} = \left| x_{\left|\frac{\partial u_s}{\partial x}=\min\left(\frac{\partial u_s}{\partial x}\right)\right.} - x_{\left|\frac{\partial u_s}{\partial x}=\max\left(\frac{\partial u_s}{\partial x}\right)\right.} \right|. \tag{3}$$

## 2.2 Theories

The weakly nonlinear ISW models we used are the KdV, JKKD, BO, and eKdV equations. For strongly nonlinear ISWs models, we consider the MCC and DJL equations (see Text S1).

The wave-induced velocity used for quantifying surface divergence can be determined by the stream function (Stastna & Peltier, 2005) :

$$\psi(x,z) = c\eta(x,z). \tag{4}$$

For a given waveform $\eta(x)$, the solution of the induced horizontal velocity under weakly nonlinear conditions has the following separable form, in which the vertical modes are independent of the horizontal location:

$$u(x,z) = \frac{\partial \psi(x,z)}{\partial z} = c_0 \eta(x) \frac{\partial \phi_b(z)}{\partial z}, \tag{5}$$

where $c_0$ is the linear phase speed and $\phi_b(z)$ is obtained by solving the Sturm–Liouville equation, written as:

$$\left(\frac{d^2}{dz^2} + \frac{N_b^2(z)}{c_0^2}\right)\phi_b(z) = 0 \qquad \phi_b(-H) = \phi_b(0) = 0, \tag{6}$$

where $N_b(z)$ is the given background buoyancy frequency, calculated by:

$$N_b^2(z) = -\frac{g}{\rho_0}\frac{d\rho(z)}{dz}, \tag{7}$$

where $g$ is the gravitational acceleration, $\rho(z)$ is the density profile, and $\rho_0$ is the reference density.

If strong nonlinearity is considered, the isopycnal displacement caused by ISWs should be considered when calculating the vertical structure. Therefore, the vertical structure function should depend on $x$ as well (Apel, 2003). The solution of the induced horizontal velocity is calculated in the following inseparable form:

$$u(x,z) = c\eta(x) \frac{\partial \phi_{wave}(x,z)}{\partial z}, \tag{8}$$

where $\phi_{wave}(x,z)$ is the vertical structure function of strongly nonlinear ISWs, calculated by iterating the changed stratification and $\eta(x,z)$ with the initial value of $\eta(x)$ (see Text S2).

# 3 Results

## 3.1 Separability of the solution of wave-induced velocity

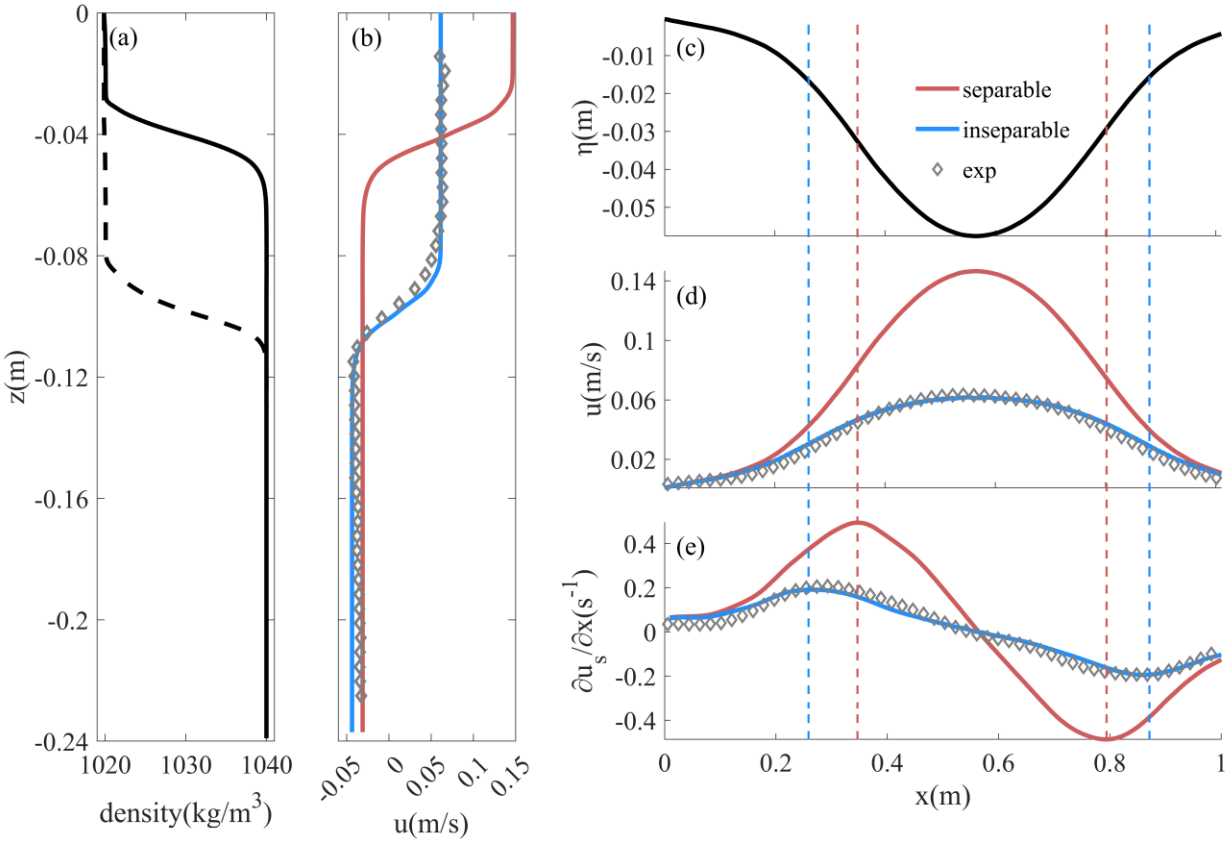


**Figure 2.** Experimental results with $h_2/h_1$=5, $\eta_0/h_1 = 1.44$. (a) The solid black line is the background density profile measured by the conductivity probe, and the dashed line is the density profile at the wave crest calculated by iteration. (b) Horizontal velocity profile at the crest, the red line, blue line, and diamond are the velocities in the separable form, inseparable form, and experiment, respectively. The legend is the same in (b, d, e). (c) Waveform. (d) Surface horizontal velocity, (e) Divergence of horizontal velocity at the surface. The red and blue dashed lines indicate the horizontal positions where the divergences reach peaks.

To visually show the influence of strong nonlinearity on the structure of wave-induced velocities, here we take a case of $h_2/h_1$=5 and $\eta_0/h_1$ =1.44 as an example in which the amplitude is of the same magnitude as $h_1$ and shows significant nonlinearity. In terms of horizontal velocity magnitude and structure, there are differences between the velocity solutions in separable (Eq.5) and inseparable (Eq.8) forms (Figure 2b and 2d). The PIV measurements

match the velocity solution in inseparable form well in both the magnitude and the structure. In the upper layer, the solution of velocity in separable form is more than twice the inseparable form, while they are closer in the lower layer. This difference between observations and theoretical solutions in separable form was also observed in the ocean, see Fig.13 of Rong et al. (2023). This can be explained by the flow conservation that the influence of ISWs on the stratification changed the thickness of the upper and lower layers. Figure 2e shows the distances of divergence peaks, where the distance in inseparable form is larger. The differences reach a maximum of 33% in the case of $\eta_0/h_1 = 2.20$. In previous studies, the relationship between $D_{p-p}$ and $L_w$ can be obtained directly by calculating velocity in separable form, as $D_{p-p} = 1.32$ $L_w$ in the KdV equation, and the ratio is independent of the amplitude. However, the experimental results show that the ratio varies from 1.4 to 2.7 with increasing amplitude. The results calculated in the inseparable form are consistent with the experiments (see Figure S1). Therefore, the strong nonlinearity cannot be neglected in the velocity calculation, especially with increasing wave amplitude. In Section 3.2, only the solution in inseparable form will be used to calculate velocities.

### 3.2 Remote sensing characteristics of ISWs

The relationship between remote sensing characteristics and wave parameters will be established in this section, and the applicability of each ISW theory will be evaluated by comparing it with experimental results. Here we take two cases of $h_2/h_1$=5, $h_1$=0.04 m, and 0.08 m as examples. The results under the other stratifications are shown in Figures S2–S4. Our experiments mainly focus on the ISWs under strong nonlinearity, and the small amplitude ISWs have been fully proven to be consistent with the theoretical and experimental results in previous studies (Ostrovsky & Stepanyants, 2005).

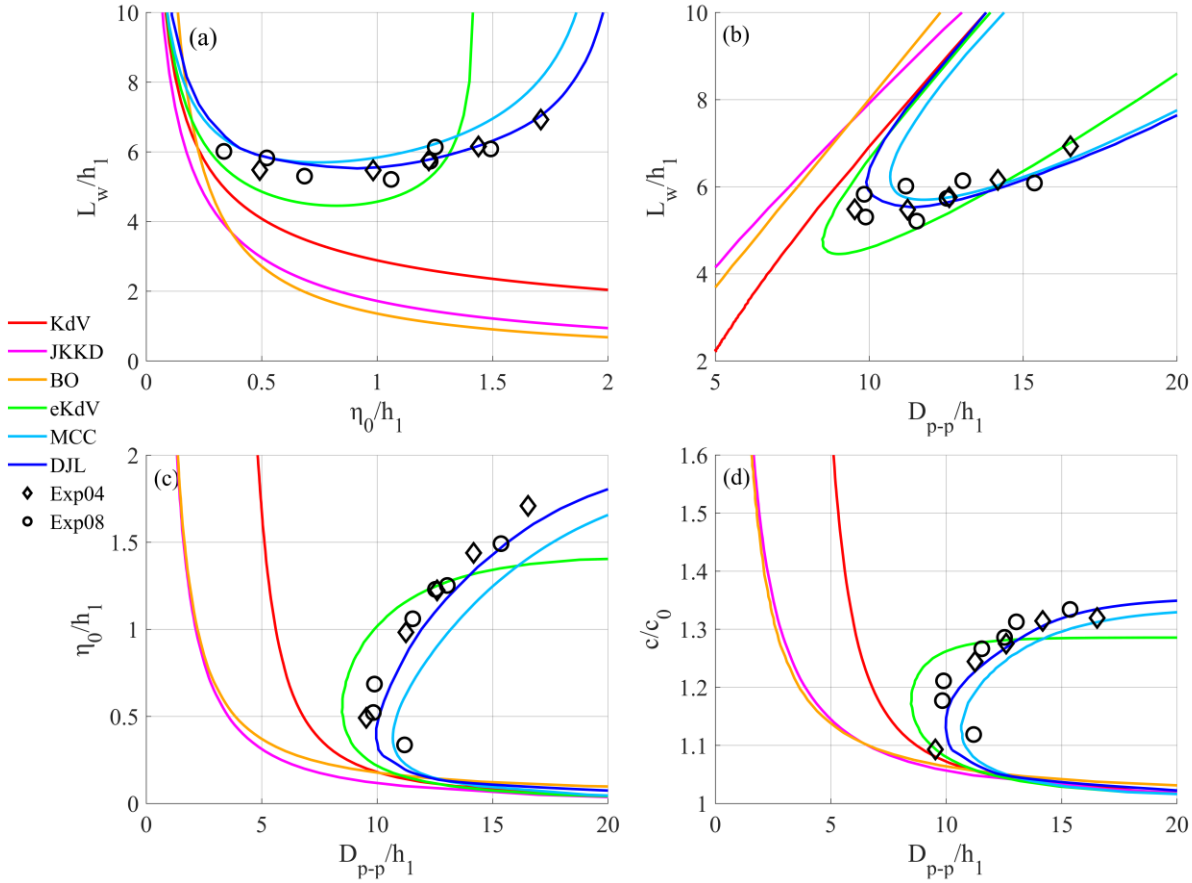


**Figure 3.** Theoretical and experimental results with $h_2/h_1$ =5, (a) the variation of $L_w$ with $\eta_0$. (b), (c), and (d) are the relationships between $D_{p-p}$ and wavelength, amplitude, and phase speed, respectively. The red, magenta, yellow, green, light blue, and dark blue lines represent the KdV, JKKD, BO, eKdV, MCC, and DJL equations respectively. The black diamond (Exp04) and the circle (Exp08) represent the experimental results for $h_1$ =0.04 m and 0.08 m, respectively.

Figures 3b-3d show the variation in wave parameters with the peak-to-peak distance $D_{p-p}$. The results from the KdV, JKKD, and BO equations show a similar pattern, in which parameters change monotonically with $D_{p-p}$. However, for the eKdV, MCC, and DJL equations, the relationship between the wave parameters and $D_{p-p}$ is no longer monotonic. Its typical feature is the existence of a turning point, which means that one $D_{p-p}$ will correspond to two parameters, that is, the existence of double solutions. The selection method for double solutions can be determined by the properties of wave packets that the leading wave reaches the maximum amplitude (Xue et al., 2013). In addition, both the eKdV equation and the fully nonlinear

equations have a limiting amplitude, which varies with different stratifications (Cui et al., 2021), and the limiting amplitude of the eKdV equation is smaller than that of the MCC and DJL equations. The comparison between the theoretical and experimental results shows that it is feasible to describe the remote sensing characteristics of ISWs with theoretical models.

To quantitatively compare the differences between ISW theories and experimental results in retrievals, we define the relative deviation (RD) as follows

$$\mathrm{RD} = \left| \frac{\lambda_{theory} - \lambda_{exp}}{\lambda_{exp}} \right| * 100\%, \tag{9}$$

where $\lambda_{theory}$ and $\lambda_{exp}$ are any theoretical and experimental parameters under a specific $D_{p-p}$. If the $D_{p-p}$ of some experiments are smaller than the theoretical minimum value, the theoretical turning point is used to calculate its RD. In Figure 4, the KdV equation is only applicable in relatively small amplitudes at any stratification. For the eKdV equation, significant RD is caused in the retrieval with dimensionless amplitude ranging between 0.5–1, corresponding to the turning point with smaller $D_{p-p}$ in this range. In addition, its limiting amplitude restricts its application at large amplitudes. Therefore, the eKdV equation is applicable to ISWs with small or nearly limiting amplitudes. For the MCC equation, the turning point gradually shifts to the direction of $D_{p-p}$ lengthening with increasing depth. The RD becomes larger with the gradual failure of the long wave assumption. The DJL equation has great applicability in all conditions. In laboratory conditions, the RD of wavelength and phase speed are less than 10% in retrievals, and the RD of small amplitude is approximately 30% which is mainly caused by the relative magnitude of variation, measurement errors, and dissipations, while RD of other amplitude is reduced to 10%.

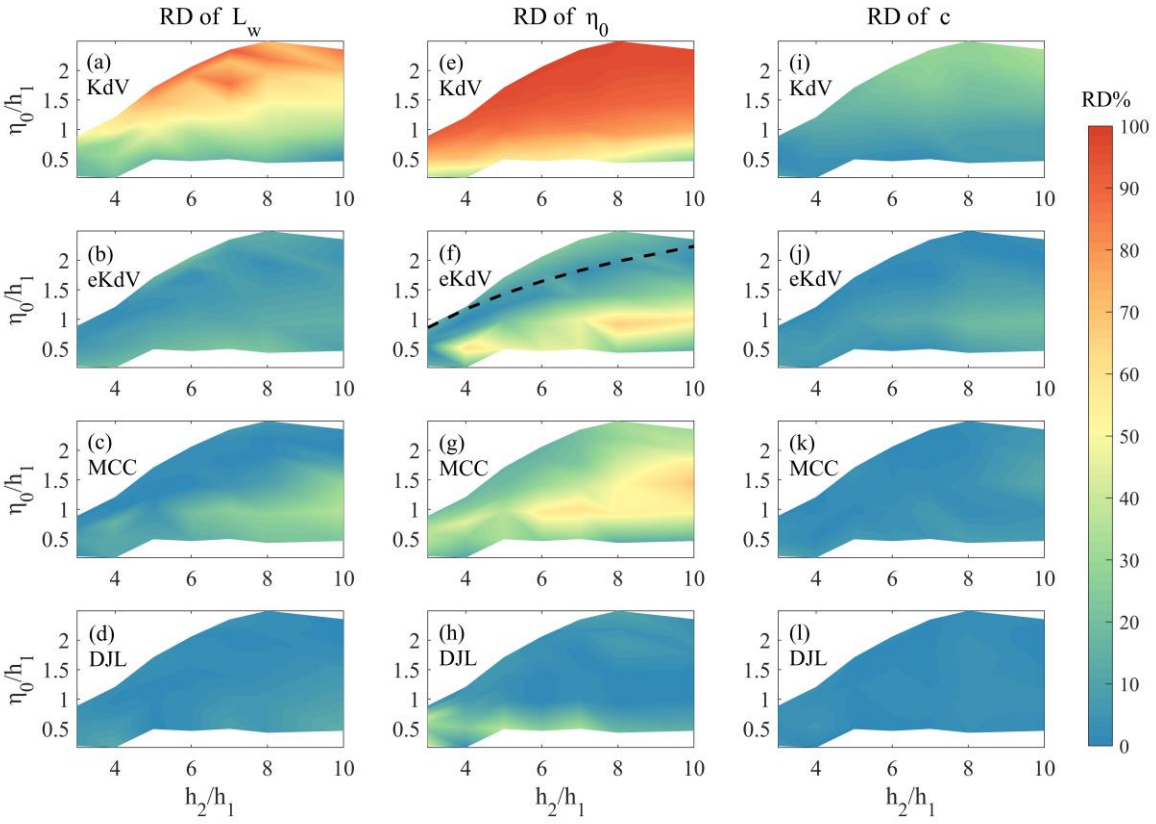


**Figure 4.** RD between theoretical and experimental results in retrievals using $D_{p-p}$. (a)-(d) are RD of KdV, eKdV, MCC, and DJL equations in retrieving wavelength, (e)-(h) are RD in retrieving amplitude, and (i)-(l) are RD in retrieving phase speed. The color bar indicates RD% in each condition, and the black dashed line in (f) indicates the limiting amplitude.

## 4 Discussion

The above work explores the retrieval of wave parameters in a quasi-two-layer procedure under laboratory conditions. However, the complex environments in the ocean introduce difficulties and variety to retrieval. Therefore, the applicability of the established method is further tested with oceanic observations.

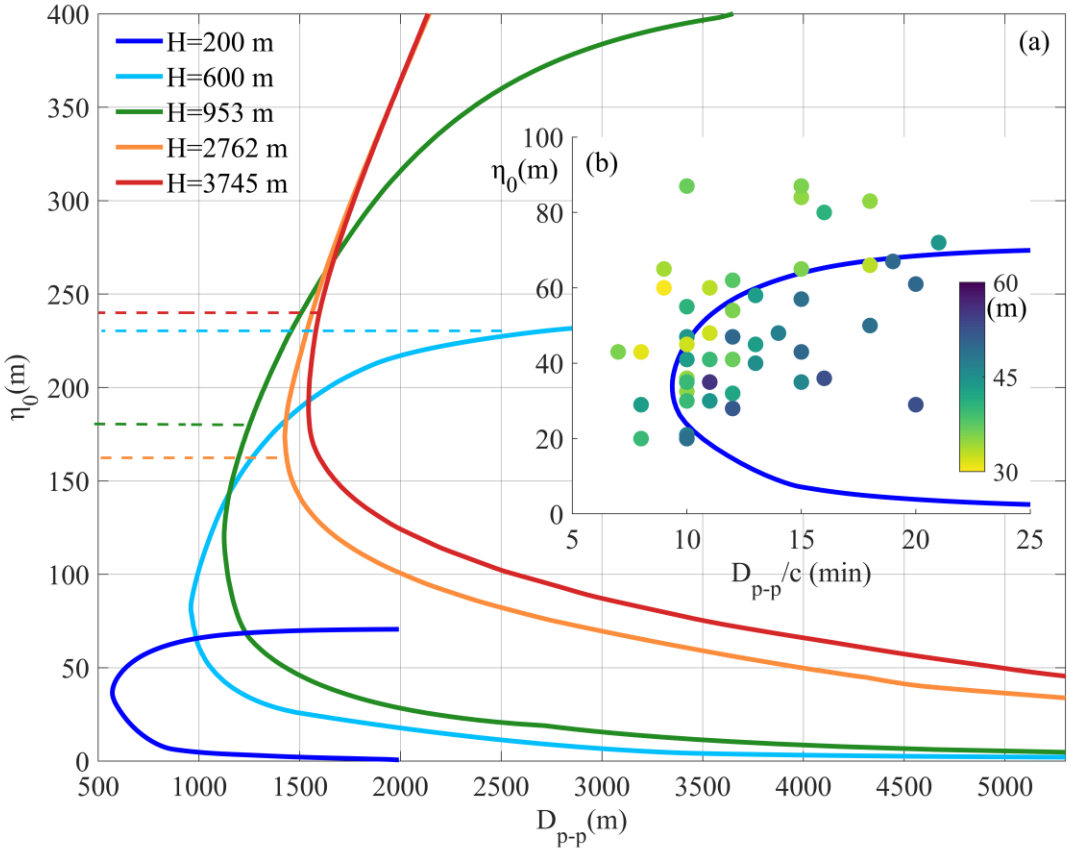


241

242 **Figure 5.** Relationship between $D_{p-p}$ and amplitude of each location calculated by the DJL
243 equation. (a) The dark line, light blue, green, orange and red lines are the results of mooring
244 stations with depths of 200 m, 600 m, 953 m, 2762 m, and 3745 m. Dashed lines of
245 corresponding colors indicate the maximum amplitude of the observed ISW at each station. (b)
246 The dark blue line is the results of stations with a depth of 200m, the dots represent the measured
247 ISWs, and their colors indicate the upper layer depth before the arrival of ISWs. The horizontal
248 axis represents the time interval of peak-to-peak in the mooring observation.

249 The results at several locations with long-term mooring are shown in Figure 5. The 200 m
250 depth is S5 during the Asian Seas International Acoustics Experiment (ASIAEX) (Duda et al.,
251 2004), the 600 m depth station is LR1 of Chang et al. (2021), and the 953 m, 2762 m, and 3745
252 m depth stations are M1, M6, and M10 of Huang et al. (2022). The yearly mean climatological
253 WOA18 dataset is used in the DJL equation except for the location of 200 m. The stratification
254 in 200 m depth is given by the average results of temperature profiles in observations before each

ISW arrives. In Figure 5b, 49 ISWs were observed during ASIAEX. The amplitude is defined as the maximum isotherm displacement. Using the time series of upward-looking ADCP with an interval of 1 min, we estimate $D_{p-p}$ by

$$D_{p-p} = c\left| t_{\left|\frac{\partial u_s}{\partial t}=\min\left(\frac{\partial u_s}{\partial t}\right)\right.} - t_{\left|\frac{\partial u_s}{\partial t}=\max\left(\frac{\partial u_s}{\partial t}\right)\right.} \right|, \tag{10}$$

and the axis is set to $D_{p-p}/c$ due to the absence of the phase speed $c$. Different from the laboratory results, the relationship between surface features and amplitudes is relatively scattered in the ocean. The amplitude will be greatly different under one condition. Even in a short period of 15 days, the upper layer depth will change between 30 m and 60 m corresponding to the amplitude difference, and this short-period change may be caused by surface forcing (Font et al., 2022). As seen from the scatter, thicker and thinner upper layers usually correspond to smaller and larger amplitudes, respectively. The amplitudes are affected by this variation in stratification over a short period, as observed by Small et al. (1999) and Lien et al. (2014). The difficulty in obtaining real-time stratification will cause errors in retrieving the parameters of a specific ISW. Nevertheless, the DJL equation using an average stratification can still reveal the trend of wave parameters with remote sensing characteristics, which will play an important role in the statistical work of the properties of ISWs using satellite images.

The curves under the measured maximum amplitude show different patterns. The amplitudes decrease approximately with the increase in $D_{p-p}$ in a deep sea of more than 2700 m. At approximately 1000 m, the amplitudes decrease monotonically except for a small area near the turning point. For the 600 m and 200 m stations, the amplitudes above the turning point will increase with increasing of $D_{p-p}$ while those below the turning point will decrease. The selection rule in the retrieval has been mentioned in Section 4.2. Different from other stations, the maximum amplitude observed at 200 m exceeds the limitation calculated by averaged stratification, which may be caused by variations in the upper layer and the shoaling of ISWs. The relationship between the remote sensing characteristics and the wave parameters of ISWs is different at those stations. In fact, the calculation results of the DJL equation under several stratifications indicate that the different stratification characteristics in different areas are the main factors that cause the differences in the retrievals, such as shallow waters with quasi-two-layer stratifications and deep seas with a main thermocline that spans hundreds of meters.

Stratification plays a critical role in the retrieval of ISW parameters from satellite images. In shallow seas, the climatological dataset cannot reflect the short-period variation in stratification, and the retrieval of parameters of a specific ISW needs additional information to improve. For the deep seas, the relatively stable stratification provides us with more possibilities for accurate retrieval.

## 5 Conclusions

In this study, we establish the relationship between the surface and internal characteristics of ISWs in dimensionless laboratory experiments. The strongly nonlinear effects of ISWs in the retrieval of wave parameters are evaluated, and a fully nonlinear model is applied in oceans. Strong nonlinearity causes the solution of the wave-induced velocity to be inseparable, and an iterative method for calculating the velocity solution in inseparable form is proposed and fits well with the experimental results. The difference in the retrieval between velocity solutions in separable and inseparable forms reaches a maximum of 33% in the range of our experimental parameters. ISW theories under weakly nonlinear assumptions have difficulty describing strongly nonlinear ISWs from the surface. The fully nonlinear DJL equation is used in the retrieval and compared with experimental results. The relative deviation of the retrieval of wavelength, amplitude, and phase speed is less than 10% in laboratory experiments except in small amplitude conditions.

The determination of ISW parameters from satellite images in oceans is significantly affected by in-situ stratifications. The variation in stratification over a short period can bring errors in retrieving the parameters of a specific ISW. However, the comparison of observations and theory shows that the DJL equation using background stratifications can reveal reasonable internal characteristics of ISWs from surface features. Stratification conditions make the relationship between remote sensing signatures and ISW parameters differ in deep and shallow seas. The amplitudes of ISWs decrease monotonically with increasing $D_{p-p}$ in deep seas, but double solutions should be considered in shallow seas.

This work provides a reliable hydrodynamics model for the inversion of remote sensing signatures of ISWs into characteristics in the ocean interior. With the combination of the fully nonlinear model and the satellite imaging mechanism, more underwater information can be interpreted from remote sensing in further work.

## Acknowledgments

The study was supported by the National Natural Science Foundation of China through grant 41876015 and the National Key Research and Development Program of China through grant 2021YFC3101603.

The author would like to thank Dr. Michael Dunphy for the solver of the DJL equation (https://github.com/mdunphy/DJLES).

## Open Research

The dataset of laboratory experiments is available at: https://doi.org/10.5281/zenodo.7636122.

## References

Alford, M. H., Peacock, T., MacKinnon, J. A., Nash, J. D., Buijsman, M. C., Centurioni, L. R., Chao, S. Y., Chang, M. H., Farmer, D. M., Fringer, O. B., Fu, K. H., Gallacher, P. C., Graber, H. C., Helfrich, K. R., Jachec, S. M., Jackson, C. R., Klymak, J. M., Ko, D. S., Jan, S., . . . Tang, T. Y. (2015). The formation and fate of internal waves in the South China Sea. *Nature*, *521*(7550), 65-69. https://doi.org/10.1038/nature14399

Alpers, W. (1985). Theory of radar imaging of internal waves. *Nature*, *314*(6008), 245-247. https://doi.org/10.1038/314245a0

Apel, J. R. (2003). A New Analytical Model for Internal Solitons in the Ocean. *Journal of Physical Oceanography*, *33*(11), 2247-2269. https://doi.org/10.1175/1520-0485(2003)033<2247:Anamfi>2.0.Co;2

Brandt, P., Romeiser, R., & Rubino, A. (1999). On the determination of characteristics of the interior ocean dynamics from radar signatures of internal solitary waves. *Journal of Geophysical Research: Oceans*, *104*(C12), 30039-30045. https://doi.org/10.1029/1999jc900092

Camassa, R., Choi, W., Michallet, H., RusÅS, P. O., & Sveen, J. K. (2006). On the realm of validity of strongly nonlinear asymptotic approximations for internal waves. *Journal of Fluid Mechanics*, *549*(-1). https://doi.org/10.1017/s0022112005007226

Camassa, R., Hurley, M. W., McLaughlin, R. M., Passaggia, P. Y., & Thomson, C. F. C. (2018). Experimental investigation of nonlinear internal waves in deep water with miscible fluids. *Journal of Ocean Engineering and Marine Energy*, *4*(4), 243-257. https://doi.org/10.1007/s40722-018-0119-9

Chang, M. H., Lien, R. C., Lamb, K. G., & Diamessis, P. J. (2021). Long‐Term Observations of Shoaling Internal Solitary Waves in the Northern South China Sea. *Journal of Geophysical Research: Oceans*, *126*(10). https://doi.org/10.1029/2020jc017129

Chen, G.-Y., Su, F.-C., Wang, C.-M., Liu, C.-T., & Tseng, R.-S. (2011). Derivation of internal solitary wave amplitude in the South China Sea deep basin from satellite images. *Journal of Oceanography*, *67*(6), 689-697. https://doi.org/10.1007/s10872-011-0073-9

Chiu, L. Y., Reeder, D. B., Chang, Y. Y., Chen, C. F., Chiu, C. S., & Lynch, J. F. (2013). Enhanced acoustic mode coupling resulting from an internal solitary wave approaching the shelfbreak in the South China Sea. *J Acoust Soc Am*, *133*(3), 1306-1319. https://doi.org/10.1121/1.4789358

Choi, W., & Camassa, R. (1999). Fully nonlinear internal waves in a two-fluid system. *Journal of Fluid Mechanics*, *396*, 1-36. https://doi.org/10.1017/s0022112099005820

Cui, J., Dong, S., & Wang, Z. (2021). Study on applicability of internal solitary wave theories by theoretical and numerical method. *Applied Ocean Research*, *111*. https://doi.org/10.1016/j.apor.2021.102629

Dalziel, S. B., Carr, M., Sveen, J. K., & Davies, P. A. (2007). Simultaneous synthetic schlieren and PIV measurements for internal solitary waves. *Measurement Science and Technology*, *18*(3), 533-547. https://doi.org/10.1088/0957-0233/18/3/001

Duda, T. F., Lynch, J. F., Irish, J. D., Beardsley, R. C., Ramp, S. R., Chiu, C. S., Tang, T. Y., & Yang, Y. J. (2004). Internal Tide and Nonlinear Internal Wave Behavior at the Continental Slope in the Northern South China Sea. *IEEE Journal of Oceanic Engineering*, *29*(4), 1105-1130. https://doi.org/10.1109/joe.2004.836998

Fan, K., Fu, B., Gu, Y., Yu, X., Liu, T., Shi, A., Xu, K., & Gan, X. (2015). Internal wave parameters retrieval from space-borne SAR image. *Frontiers of Earth Science*, *9*(4), 700-708. https://doi.org/10.1007/s11707-015-0506-7

Font, E., Queste, B. Y., & Swart, S. (2022). Seasonal to Intraseasonal Variability of the Upper Ocean Mixed Layer in the Gulf of Oman. *Journal of Geophysical Research: Oceans*, *127*(3). https://doi.org/10.1029/2021jc018045

Gong, Y., Xie, J., Xu, J., Chen, Z., He, Y., & Cai, S. (2021). Oceanic internal solitary waves at the Indonesian submarine wreckage site. *Acta Oceanologica Sinica*, *41*(3), 109-113. https://doi.org/10.1007/s13131-021-1893-0

Helfrich, K. R., & Melville, W. K. (2006). Long Nonlinear Internal Waves. *Annual Review of Fluid Mechanics*, *38*(1), 395-425. https://doi.org/10.1146/annurev.fluid.38.050304.092129

Hong, D.-B., Yang, C.-S., & Ouchi, K. (2016). Preliminary study of internal solitary wave amplitude off the East coast of Korea based on synthetic aperture radar data. *Journal of Marine Science and Technology*, *24*(6), 17. https://doi.org/10.6119/JMST-016-1026-8

Huang, X., Chen, Z., Zhao, W., Zhang, Z., Zhou, C., Yang, Q., & Tian, J. (2016). An extreme internal solitary wave event observed in the northern South China Sea. *Sci Rep*, *6*, 30041. https://doi.org/10.1038/srep30041

Huang, X., Huang, S., Zhao, W., Zhang, Z., Zhou, C., & Tian, J. (2022). Temporal variability of internal solitary waves in the northern South China Sea revealed by long-term mooring observations. *Progress in Oceanography*, *201*. https://doi.org/10.1016/j.pocean.2021.102716

Jackson, C. (2007). Internal wave detection using the Moderate Resolution Imaging Spectroradiometer (MODIS). *Journal of Geophysical Research*, *112*(C11). https://doi.org/10.1029/2007jc004220

Jia, T., Liang, J., Li, X.-M., & Fan, K. (2019). Retrieval of internal solitary wave amplitude in shallow water by tandem spaceborne SAR. *Remote Sensing*, *11*(14), 1706. https://doi.org/https://doi.org/10.3390/rs11141706

Klymak, J. M., Pinkel, R., Liu, C. T., Liu, A. K., & David, L. (2006). Prototypical solitons in the South China Sea. *Geophysical Research Letters*, *33*(11). https://doi.org/10.1029/2006gl025932

Kodaira, T., Waseda, T., Miyata, M., & Choi, W. (2016). Internal solitary waves in a two-fluid system with a free surface. *Journal of Fluid Mechanics*, *804*, 201-223. https://doi.org/10.1017/jfm.2016.510

Lenain, L., & Pizzo, N. (2021). Modulation of surface gravity waves by internal waves. *Journal of Physical Oceanography*. https://doi.org/10.1175/jpo-d-20-0302.1

Lien, R.-C., Henyey, F., Ma, B., & Yang, Y. J. (2014). Large-Amplitude Internal Solitary Waves Observed in the Northern South China Sea: Properties and Energetics. *Journal of Physical Oceanography*, *44*(4), 1095-1115. https://doi.org/10.1175/jpo-d-13-088.1

Liu, B., Yang, H., Zhao, Z., & Li, X. (2014). Internal solitary wave propagation observed by tandem satellites. *Geophysical Research Letters*, *41*(6), 2077-2085. https://doi.org/10.1002/2014gl059281

Luzzatto-Fegiz, P., & Helfrich, Karl R. (2014). Laboratory experiments and simulations for solitary internal waves with trapped cores. *Journal of Fluid Mechanics*, *757*, 354-380. https://doi.org/10.1017/jfm.2014.501

Moum, J. N., Farmer, D. M., Smyth, W. D., Armi, L., & Vagle, S. (2003). Structure and Generation of Turbulence at Interfaces Strained by Internal Solitary Waves Propagating Shoreward over the Continental Shelf. *Journal of Physical Oceanography*, *33*(10), 2093-2112. https://doi.org/10.1175/1520-0485(2003)033<2093:Sagota>2.0.Co;2

Osborne, A. R., & Burch, T. L. (1980). Internal solitons in the andaman sea. *Science*, *208*(4443), 451-460. https://doi.org/10.1126/science.208.4443.451

Ostrovsky, L. A., & Stepanyants, Y. A. (2005). Internal solitons in laboratory experiments: comparison with theoretical models. *Chaos*, *15*(3), 37111. https://doi.org/10.1063/1.2107087

Pan, J., Jay, D. A., & Orton, P. M. (2007). Analyses of internal solitary waves generated at the Columbia River plume front using SAR imagery. *Journal of Geophysical Research*, *112*(C7). https://doi.org/10.1029/2006jc003688

Phaniharam, S. A., Chintam, V., Baggu, G., & Koneru, V. S. R. P. (2020). Study of internal wave characteristics off northwest Bay of Bengal using synthetic aperture radar. *Natural Hazards*, *104*(3), 2451-2460. https://doi.org/10.1007/s11069-020-04280-6

Ramp, S. R., Yang, Y. J., & Bahr, F. L. (2010). Characterizing the nonlinear internal wave climate in the northeastern South China Sea. *Nonlinear Processes in Geophysics*, *17*(5), 481-498. https://doi.org/10.5194/npg-17-481-2010

Romeiser, R., & Graber, H. C. (2015). Advanced Remote Sensing of Internal Waves by Spaceborne Along-Track InSAR—A Demonstration With TerraSAR-X. *IEEE Transactions on Geoscience and Remote Sensing*, *53*(12), 6735-6751. https://doi.org/10.1109/tgrs.2015.2447547

Rong, L., Xiong, X., & Chen, L. (2023). Assessment of KdV and EKdV theories for simulating internal solitary waves in the continental slope of the South China Sea. *Continental Shelf Research*. https://doi.org/10.1016/j.csr.2023.104944

Small, J., Hallock, Z., Pavey, G., & Scott, J. (1999). Observations of large amplitude internal waves at the Malin Shelf edge during SESAME 1995. *Continental Shelf Research*, *19*(11), 1389-1436. https://doi.org/10.1016/s0278-4343(99)00023-0

Stanton, T. P., & Ostrovsky, L. A. (1998). Observations of highly nonlinear internal solitons over the continental shelf. *Geophysical Research Letters*, *25*(14), 2695-2698. https://doi.org/10.1029/98gl01772

Stastna, M., & Peltier, W. R. (2005). On the resonant generation of large-amplitude internal solitary and solitary-like waves. *Journal of Fluid Mechanics*, *543*(-1). https://doi.org/10.1017/s002211200500652x

Sutherland, B., Keating, S., & Shrivastava, I. (2015). Transmission and reflection of internal solitary waves incident upon a triangular barrier. *Journal of Fluid Mechanics*, *775*, 304-327. https://doi.org/https://doi.org/10.1017/jfm.2015.306

Thielicke, W., & Stamhuis, E. J. (2014). PIVlab – Towards User-friendly, Affordable and Accurate Digital Particle Image Velocimetry in MATLAB. *Journal of Open Research Software*, *2*. https://doi.org/10.5334/jors.bl

Vlasenko, V., Brandt, P., & Rubino, A. (2000). Structure of Large-Amplitude Internal Solitary Waves. *Journal of Physical Oceanography*, *30*(9), 2172-2185. https://doi.org/10.1175/1520-0485(2000)030<2172:Solais>2.0.Co;2

Wang, C., Wang, X., & Da Silva, J. C. B. (2019). Studies of Internal Waves in the Strait of Georgia Based on Remote Sensing Images. *Remote Sensing*, *11*(1). https://doi.org/10.3390/rs11010096

Wang, S., Chen, X., Wang, J., Li, Q., Meng, J., & Xu, Y. (2019). Scattering of Low-Mode Internal Tides at a Continental Shelf. *Journal of Physical Oceanography*, *49*(2), 453-468. https://doi.org/10.1175/jpo-d-18-0179.1

Wang, T., Huang, X., Zhao, W., Zheng, S., Yang, Y., & Tian, J. (2022). Internal Solitary Wave Activities near the Indonesian Submarine Wreck Site Inferred from Satellite Images. *Journal of Marine Science and Engineering*, *10*(2). https://doi.org/10.3390/jmse10020197

Wang, Y.-H., Dai, C.-F., & Chen, Y.-Y. (2007). Physical and ecological processes of internal waves on an isolated reef ecosystem in the South China Sea. *Geophysical Research Letters*, *34*(18). https://doi.org/10.1029/2007gl030658

Xie, H., Xu, Q., Zheng, Q., Xiong, X., Ye, X., & Cheng, Y. (2022). Assessment of theoretical approaches to derivation of internal solitary wave parameters from multi-satellite images near the Dongsha Atoll of the South China Sea. *Acta Oceanologica Sinica*, *41*(6), 137-145. https://doi.org/10.1007/s13131-022-2015-3

Xue, J., Graber, H. C., Lund, B., & Romeiser, R. (2013). Amplitudes Estimation of Large Internal Solitary Waves in the Mid-Atlantic Bight Using Synthetic Aperture Radar and Marine X-Band Radar Images. *IEEE Transactions on Geoscience and Remote Sensing*, *51*(6), 3250-3258. https://doi.org/10.1109/tgrs.2012.2221467

Yang, Y., Huang, X., Zhao, W., Zhou, C., Huang, S., Zhang, Z., & Tian, J. (2021). Internal Solitary Waves in the Andaman Sea Revealed by Long-Term Mooring Observations. *Journal of Physical Oceanography*, *51*(12), 3609-3627. https://doi.org/https://doi.org/10.1175/JPO-D-20-0310.1

Yue, L., Hao, X., Shen, L., & Fringer, O. B. (2022). Direct Simulation of the Surface Manifestation of Internal Gravity Waves with a Wave-Current Interaction Model. *Journal of Physical Oceanography*. https://doi.org/10.1175/jpo-d-22-0097.1

Zhao, Z., Klemas, V., Zheng, Q., & Yan, X.-H. (2004). Remote sensing evidence for baroclinic tide origin of internal solitary waves in the northeastern South China Sea. *Geophysical Research Letters*, *31*(6), n/a-n/a. https://doi.org/10.1029/2003gl019077

Zheng, Q., Yuan, Y., Klemas, V., & Yan, X.-H. (2001). Theoretical expression for an ocean internal soliton synthetic aperture radar image and determination of the soliton characteristic half width. *Journal of Geophysical Research: Oceans*, *106*(C12), 31415-31423. https://doi.org/10.1029/2000jc000726

**References from the Supporting Information**

Benjamin, T. B. (1967). Internal waves of permanent form in fluids of great depth. *Journal of Fluid Mechanics*, *29*(3), 559-592. https://doi.org/https://doi.org/10.1017/S002211206700103X

Camassa, R., Choi, W., Michallet, H., RusÅS, P. O., & Sveen, J. K. (2006). On the realm of validity of strongly nonlinear asymptotic approximations for internal waves. *Journal of Fluid Mechanics*, *549*(-1). https://doi.org/10.1017/s0022112005007226

Choi, W., & Camassa, R. (1999). Fully nonlinear internal waves in a two-fluid system. *Journal of Fluid Mechanics*, *396*, 1-36. https://doi.org/10.1017/s0022112099005820

Dunphy, M., Subich, C., & Stastna, M. (2011). Spectral methods for internal waves: indistinguishable density profiles and double-humped solitary waves. *Nonlinear Processes in Geophysics*, *18*(3), 351-358. https://doi.org/10.5194/npg-18-351-2011

Grimshaw, R., Pelinovsky, E., Talipova, T., & Kurkin, A. (2004). Simulation of the Transformation of Internal Solitary Waves on Oceanic Shelves. *Journal of Physical Oceanography*, *34*(12), 2774-2791. https://doi.org/10.1175/jpo2652.1

Kakutani, T., & Yamasaki, N. (1978). Solitary Waves on a Two-Layer Fluid. *Journal of the Physical Society of Japan*, *45*(2), 674-679. https://doi.org/10.1143/jpsj.45.674

Korteweg, D. J., & de Vries, G. (1895). XLI. On the change of form of long waves advancing in a rectangular canal, and on a new type of long stationary waves. *The London, Edinburgh, and Dublin Philosophical Magazine and Journal of Science*, *39*(240), 422-443. https://doi.org/10.1080/14786449508620739

Long, R. R. (1953). Some Aspects of the Flow of Stratified Fluids: I. A Theoretical Investigation. *Tellus*, *5*(1), 42-58. https://doi.org/10.3402/tellusa.v5i1.8563

Miyata, M. (1988). Long internal waves of large amplitude. In *Nonlinear water waves* (pp. 399-406). Springer. https://doi.org/10.1007/978-3-642-83331-1_44

Ono, H. (1975). Algebraic Solitary Waves in Stratified Fluids. *Journal of the Physical Society of Japan*, *39*(4), 1082-1091. https://doi.org/10.1143/jpsj.39.1082

Stastna, M., & Lamb, K. G. (2002). Large fully nonlinear internal solitary waves: The effect of background current. *Physics of Fluids*, *14*(9), 2987-2999. https://doi.org/10.1063/1.1496510

Zheng, Q., Yan, X.-H., & Klemas, V. (1993). Statistical and dynamical analysis of internal waves on the continental shelf of the Middle Atlantic Bight from space shuttle photographs. Journal of Geophysical Research: Oceans, 98(C5), 8495-8504. https://doi.org/10.1029/92jc02955